3-D Reflectarray Antenna Design for Ku Application Using 3-D Printer Technology

IEEE Access
Multidisciplinary : Rapid Review : Open Access Journal

Received 10 May 2026, accepted 24 May 2026, date of publication 5 June 2026, date of current version 11 June 2026.

Digital Object Identifier 10.1109/ACCESS.2026.3700326

RESEARCH ARTICLE

3-D Reflectarray Antenna Design for Ku Application Using 3-D Printer Technology

LADISLAU MATEKOVITS [1,2,3], (Senior Member, IEEE), FURKAN BAŞKıR [4], HASAN KıYıK [5], AYSU BELEN [6], TARLAN MAHOUTI [7], AND MEHMET ALI BELEN [4]

[1]Department of Electronics and Telecommunications, Politecnico di Torino, 10129 Turin, Italy
[2]Istituto di Elettronica e di Ingegneria dell'Informazione e delle Telecomunicazioni, National Research Council of Italy, 10129 Turin, Italy
[3]Faculty of Electronics and Telecommunications, Politehnica University Timişoara, 300006 Timişoara, Romania
[4]Department of Electric and Electronical Engineering, İskenderun Technical University, 31200 İskenderun, Hatay, Türkiye
[5]Turkish Aerospace Industries, 26003 İstanbul, Türkiye
[6]Department of Hybrid and Electric Vehicles, İskenderun Technical University, 31200 İskenderun, Hatay, Türkiye
[7]Department of Metallurgical and Materials Engineering, Yıldız Technical University, 34349 İstanbul, Türkiye

Corresponding author: Ladislau Matekovits (ladislau.matekovits@polito.it)

This work was supported in part by Yıldız Technical University under Project FBA-2025-6780, and in part by Turkish Aerospace Industries through the Turkish Aerospace Industries Inc (TAI) Lift Up Industry-Oriented Undergraduate Capstone Projects Program titled "Design of a Reconfigurable Intelligent Surface (RIS) for Radar Cross-Section Reduction in Aerospace Applications" under Project 68AB317641672.

ABSTRACT This paper presents the design, fabrication, and experimental validation of a Ku-band 3D-printed reflectarray (RA) antenna established on a quasi-periodic arrangement, operating at 13 GHz. The proposed grounded dielectric 3D unit cell consists of a polylactic acid (PLA)-based multilayer structure incorporating a constant height prism on top of which a variable height square prism resonator is located; such a configuration is maintained at a constant distance from the ground plane by an air spacer. The arrangement enables continuous reflection-phase control through geometry and material parameter tuning. A systematic parametric analysis is conducted to quantify the influence of air-gap thickness, dielectric thickness, relative permittivity, and resonator dimensions on the reflection-phase response. The results demonstrate that the air spacer provides the dominant phase-adjustment mechanism, while the remaining parameters enable fine-resolution phase compensation, forming a practical and fabrication-aware phase-synthesis strategy. Using full-wave–generated phase mapping and classical RA compensation principles, a 16×16 array comprising 256 elements with an aperture size of 240×240 mm^2 is synthesized. The simulated and measured maximum gains at 13 GHz are 22.8 dBi and 21.4 dBi, respectively, with controlled sidelobe levels and stable main-beam polarization characteristics, while the corresponding aperture efficiency is 10.2%. A prototype has been fabricated using additive manufacturing technology and experimentally characterized in a horn-fed measurement setup. The measured radiation characteristics show good agreement with simulations, validating both the unit-cell model and the aperture-level phase distribution methodology. The proposed approach demonstrates that low-cost 3D-printing technology can realize high-gain Ku-band RAs without multilayer stacking or complex fabrication processes. Owing to its scalability, lightweight structure, and compatibility with tunable elements, the presented design framework offers a promising pathway toward broadband, reconfigurable RAs and next-generation intelligent reflecting surfaces for satellite and high-frequency wireless communication applications.

INDEX TERMS Reflectarray, antenna design, Ku-band, 3-D printer.

I. INTRODUCTION

Reflectarray (RA) antennas have emerged as a compelling high-gain solution by combining the aperture efficiency of reflector antennas with the wavefront-shaping capability of phased arrays [1]. An RA typically consists of a planar or mildly curved surface of (quasi-)periodic unit cells illuminated by a feed, where each cell is engineered to provide a prescribed reflection phase so that the overall aperture transforms the incident spherical wave into a desired radiated

The associate editor coordinating the review of this manuscript and approving it for publication was Ravi Kumar Gangwar.

beam [2], [3]. Owing to their low profile, reduced mass, and versatility in beam shaping (including contoured or multi-beam coverage), RAs have been widely investigated for satellite and high-capacity wireless systems [4].

The Ku-band remains a particularly relevant frequency range for satellite communications, including Very-small-aperture terminal (VSAT), direct-broadcast services, and transportable emergency links, where compact high-gain antennas are required under stringent cost and form-factor constraints [5]. However, achieving wide bandwidth, high efficiency in Ku-band RAs is challenged by the phase range and dispersion of the unit cells, conductor/dielectric losses, and manufacturing tolerances [6].

Recently, additive manufacturing (3D printing) has gained momentum as an enabling fabrication route for high-frequency apertures, offering rapid prototyping, reduced part count via monolithic architectures, and new degrees of freedom for metal-only or full dielectric RA implementations [7], [8], [9], [10]. Building on these trends, this work focuses on the design and fabrication of a Ku-band 3D RA antenna using 3D printer technology, targeting a cost-effective, time efficient and digitally controlled manufacturable architecture while maintaining competitive radiation performance.

II. DESIGN OF UNIT ELEMENT

A RA antenna forms a high-gain aperture by illuminating a planar (or slightly curved) surface of (quasi-)periodic reflective unit cells with a feed, typically a horn (Figure 1). The feed generates a spherical wavefront, and the RA converts it into the desired radiated field by imposing a prescribed spatial distribution of reflection phase across the surface. In practice, each unit cell is designed so that its reflection coefficient provides (i) the required phase value at its location to compensate the feed path and synthesize the target beam direction or coverage, and (ii) a high reflection magnitude to preserve aperture efficiency. Consequently, unit-cell design is a central step in RA development and is commonly assessed in terms of phase range, loss, bandwidth, polarization behaviour, and robustness to practical illumination and fabrication effects [3], [11].

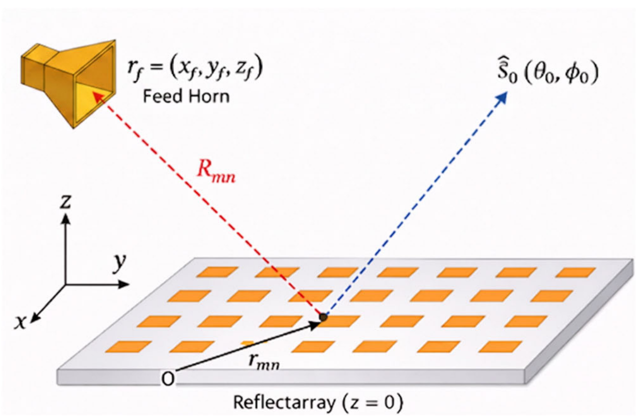

FIGURE 1. Conceptual illustration of a reflectarray.

From a unit-cell perspective, one of the primary requirements is achieving a sufficiently wide and controllable reflection-phase range—ideally approaching 360°—with a smooth and preferably monotonic dependence on the geometrical tuning parameter (e.g., patch size, slot length, or 3D feature dimensions) [12]. The presence of such feature/characteristic/possibility simplifies phase synthesis and reduces sensitivity to manufacturing deviations. Bandwidth is another key constraint because many unit-cell topologies are resonant and therefore exhibit dispersive phase behaviour; for wideband operation, designers typically seek phase responses that remain usable over the intended frequency span, either by using multi-resonant/multi-layer concepts or by adopting elements with reduced phase dispersion [13], [14]. In addition, the unit cell must meet polarization requirements (linear or circular, single or dual polarization) while maintaining low cross-polarization; for dual-polarized designs, independent and stable phase control along orthogonal field components is often necessary. These considerations are particularly relevant when 3D printing is used, because printing resolution, layer-induced stair-stepping, dimensional tolerances, and material-property variability can shift resonances and perturb phase responses; therefore, sensitivity to tolerances and manufacturability constraints should be incorporated properly in the unit-cell design process.

In this study, a Polylactic Acid (PLA) - based multilayer unit-cell geometry is proposed for reflector antenna applications. The schematic representation of the unit cell is given in Fig. 2. In the side (cross-sectional) view in Fig. 2(a), a conductive copper layer is located at the bottom, followed by an air spacer layer, and a PLA dielectric layer on top. In addition, a PLA post/protrusion placed on the PLA layer enables adjustment of the overall height and the effective electromagnetic loading of the cell. The top view in Fig. 2(b) shows a square-ring–type resonator defined on the copper layer, where the periodic dimension of the unit cell (W1) and the inner opening are controlled through the design parameters, i.e., W2 and H3.

The main geometric and material variables defining the unit cell are as follows: H1 (PLA base thickness), H2 (air spacer thickness), H3 (PLA post height), W1 (unit-cell/resonator outer size—period/outer side length), W2 (inner opening/inner size of the resonator), and εr (relative permittivity of PLA). The sweep ranges and step sizes of these parameters are summarized in Tab. 1. Here, W1 is kept fixed due to design constraints (periodicity and the target band/scale requirements), while the remaining parameters are swept parametrically within the specified intervals.

To validate the proposed design and identify the parameters that most strongly influence performance, a sensitivity analysis is carried out based on full-wave electromagnetic simulations. In this framework, the impact of each variable on the unit-cell reflection characteristics (e.g., magnitude/phase of the reflection coefficient) is examined individually. Periodic boundary conditions have been used fr this analysis. Figure 3 summarizes the one-parameter-at-a-time sensitivity analysis of the proposed reflector unit cell by reporting the 3D EM simulator response of reflection phase, over the 12–14 GHz band. In each parametric sweep, only one design variable is varied within a predefined interval, while all remaining parameters are kept constant at their nominal values. This strategy enables a direct assessment of the individual contribution of each geometrical/material parameter to the unit-cell phase response. As illustrated in Fig. 3(a), the relative dielectric constant of the PLA layer (ε_r) is swept from 1.5 to 3, while H1 = 2 mm, H2 = 2 mm, H3 = 5 mm, W1 = 15 mm, and W2 = 10 mm are fixed. The results indicate a clear and monotonic phase variation with ε_r, where increasing εr produces a consistent shift in the reflection phase across the operating band. In Fig. 3(b), the air spacer thickness (H2, denoted as h) is varied from 1 mm to 3 mm while keeping $\varepsilon_r = 2.1$, H1 = 2 mm, H3 = 5 mm, W1 = 15 mm, and W2 = 10 mm constant. Compared to the other sweeps, the air-gap thickness yields the largest phase tuning range, highlighting H2 as a dominant parameter that strongly controls the effective electrical height and, consequently, the reflection phase.

More specifically, the role of H2 can be interpreted in terms of the effective electrical path between the grounded reflecting plane and the dielectric loading region. Increasing the air-spacer height modifies the phase delay accumulated by the reflected wave and therefore shifts the reflection phase almost continuously over the investigated frequency range. Although the phase curves in Fig. 3 are plotted in an unwrapped form, the reflectarray synthesis uses the phase response modulo 360°. The H2 sweep from 1 mm to 3 mm provides an unwrapped phase excursion exceeding 360° at the operating frequencies; hence, after phase wrapping, the available phase states cover the full 0°–360° interval required for aperture phase compensation. The remaining parameters, namely the PLA base thickness H1, the relative permittivity ε_r, and the in-plane resonator dimension H3, provide additional fine phase tuning, which improves the matching between the required cell-by-cell phase distribution and the realizable unit-cell responses.

Figure 3(c) presents the influence of the PLA base thickness (H1, denoted as ht), swept from 1 mm to 3 mm, with εr = 2.1, H2 = 2 mm, H3 = 5 mm, W1 = 15 mm, and W2 = 10 mm fixed. Similarly to the ε_r sweep, changing H1 leads to a systematic phase shift, indicating that the dielectric thickness provides an additional degree of freedom for phase adjustment. Finally, Fig. 3(d) shows the effect of H3 while the remaining variables are held constant ($\varepsilon_r = 2.1$, H1 = 2 mm, H2 = 2 mm, W1 = 15 mm W2=10mm). The curves confirm that the lateral geometry also enables phase control, although its influence is smaller than the air-gap thickness in the presented band. Overall, the curves in Fig. 3 exhibit a largely consistent frequency-dependent trend, while the main effect of each parameter is observed as a phase offset/tuning across the band. These results quantitatively justify the selected design variables and provide guidance for subsequent optimization of the unit cell toward the desired reflector/reflectarray phase performance.

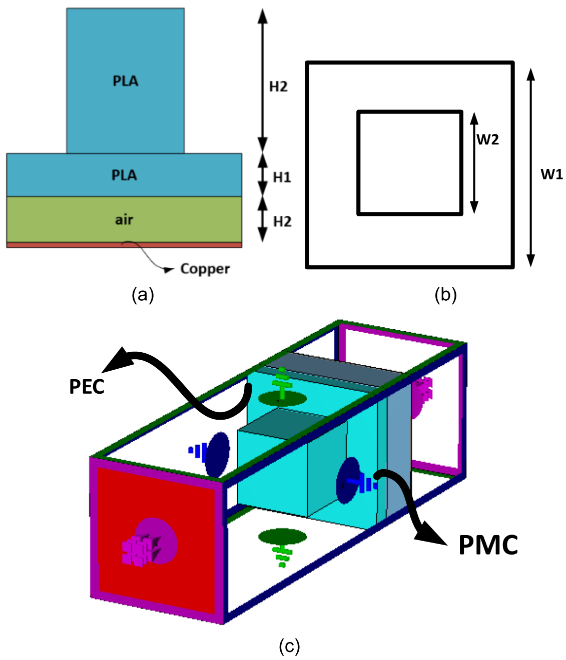

FIGURE 2. (a) Schematic view, (b) Top view, (c) 3D simulation model with boundary conditions, of the RA unit cell.

TABLE 1. Design variables of the proposed unit cell and their sweep settings used in the sensitivity analysis: parameter ranges and step sizes (H1, H2, H3, W1, and W2 in mm; ε_r is dimensionless).

Parameter	Range	Step
H1	1-5	1
H2	1-3	1
H3	1-20	1
W1	15	constant
W2	3-10	1
ε_r	1.5-3	0.25

III. MODELING AND SIMULATION OF RA

A unit-cell–based RA is designed by enforcing constructive interference of the fields scattered by all reflective cells in a prescribed far-field direction.

Let us consider a planar RA located on $z = 0$, with the mn-th cell centred at $\boldsymbol{r}_{mn}$ =(x_{mn},y_{mn},0), and a feed placed at r_f. Let (Eq. 1):

$$R_{mn} = \left\| \boldsymbol{r}_{mn} - \boldsymbol{r}_f \right\| \tag{1}$$

be the feed-to-cell distance and k_0=$2\pi/\lambda_0$ the free-space wavenumber at the design frequency f_0. The target main-beam direction is defined by $\widehat{S}_0$ (θ_0, ϕ_0) (Eq. 2) with unit vector

$$\widehat{S}_0 = (\sin\theta_0\cos\varphi_0, \sin\theta_0\sin\varphi_0, \cos\theta_0) \tag{2}$$

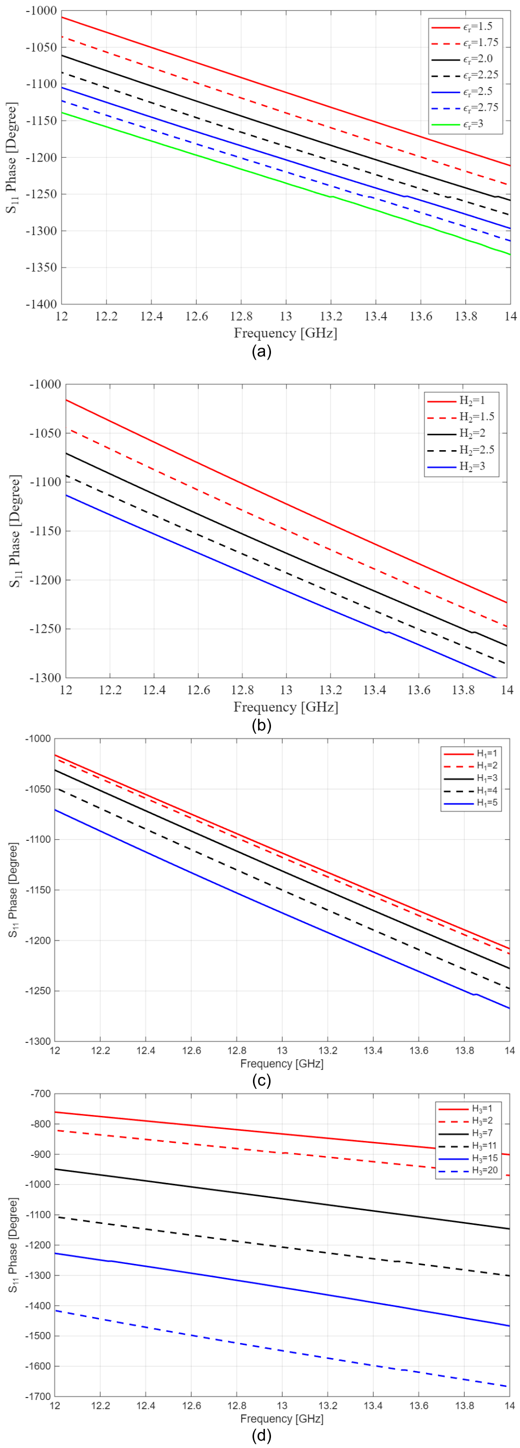

FIGURE 3. One-parameter-at-a-time sensitivity analysis of the proposed unit cell in terms of simulated unwrapped reflection phase (∠S11) over 12–14 GHz. The H2 sweep provides a phase excursion exceeding 360°, which corresponds to complete 0°–360° phase coverage after modulo-360° phase wrapping: (a) effect of PLA relative permittivity (ε_r = 1.5–3) with H1 = 2 mm, H2 = 2 mm, H3 = 5 mm, W1 = 15 mm, W2 = 10 mm fixed; (b) effect of air-gap thickness (H2 = 1–3 mm) with ε_r = 2.1, H1 = 2 mm, H3 = 5 mm, W1 = 15 mm, W2 = 10 mm fixed; (c) effect of PLA base thickness (H1 = 1–5 mm) with ε_r = 2.1, H2 = 2 mm, H3 = 5 mm, W1 = 15 mm, W2 = 10 mm fixed; (d) effect of H3 (1–20 mm) with ε_r = 2.1, H1 = 2 mm, H2 = 2 mm, W1 = 15, W2 = 10 mm fixed.

Using the standard far-field phase term $e^{-jk\widehat{S}_0.\boldsymbol{r}_{mn}}$ for radiation from location $\boldsymbol{r}_{mn}$ the total phase contribution of the mn-th element toward $\widehat{\boldsymbol{S}}_0$ can be written (up to a common constant). Enforcing equal total phase for all cells yields the required phase distribution (Eq. 3):

$$\varphi_{mn} = k_0 \left(R_{mn} + \widehat{S}_0.r_{mn}\right) + \varphi_{ref}(\mathrm{mod}(2\pi)) \tag{3}$$

where φ_{ref} is an arbitrary reference constant. (Depending on the chosen phase reference and field sign convention, the dot-product term may appear with the opposite sign; in practice, the design is implemented modulo 2π and commonly referenced to a selected cell to remove ambiguity.) For broadside beams (θ_0=0) on a planar surface, $\widehat{\boldsymbol{S}}_0.\boldsymbol{r}_{mn}$=0, and the synthesis reduces to $\phi_{\mathrm{mn}} \approx k_0 R_{\mathrm{mn}} + \phi_{\mathrm{ref}}$ [9].

After computing ϕ_{mn} over the full aperture, the design proceeds through a unit-cell characterization and mapping stage. A candidate unit-cell topology (e.g., patch, dipole, slot, multilayer stack, or metal-only 3D geometry) is simulated under periodic boundary conditions to extract its complex reflection coefficient $\Gamma(g) = |\Gamma(g)|\, e^{j\phi(g)}$ as a function of a tunable geometric parameter g (such as patch size or 3D feature height). This produces a lookup table relating geometry to reflection phase and loss at the relevant polarization(s) and incidence angles. Each RA cell is then assigned a geometry g_{mn} from the previously built lookup table so that $\phi(\mathrm{g}_{\mathrm{mn}}) \approx \phi_{\mathrm{mn}}$ while keeping $|\Gamma(\mathrm{g}_{mn})|$high. Practical implementations additionally verify phase stability under oblique incidence (since the feed illuminates the aperture with varying angles) and consider effects such as element spacing (to avoid grating lobes), mutual coupling (to assess the limits of the local periodic approximation), and fabrication tolerances.

Building upon the unit-cell concept introduced in Fig. 2, the RA antenna presented in this work is realized by mapping the required phase distribution across a large aperture through the phase response of the proposed unit cell. Specifically, the desired reflection phase at each cell location is computed using the formulation given in the preceding section, and the corresponding geometrical/material configuration of the unit cell is selected such that its simulated reflection phase matches the required value as closely as possible. In this way, a large-aperture RA is synthesized by assigning an appropriate unit-cell design to every position on the array surface.

The computed required reflection-phase distribution across the 16 × 16 reflectarray aperture is shown in Fig. 4(b). The phase values were calculated at 13 GHz using the feed-to-cell path-length compensation formulation given in Eqs. (1)–(3), and then wrapped into the 0°–360° interval for visualization. In the present center-fed broadside configuration, the aperture consists of 16 × 16 cells with a periodicity of 15 mm, and the resulting phase map is symmetric with respect to both the x- and y-axes. This computed phase distribution was used to assign the corresponding unit-cell geometries across

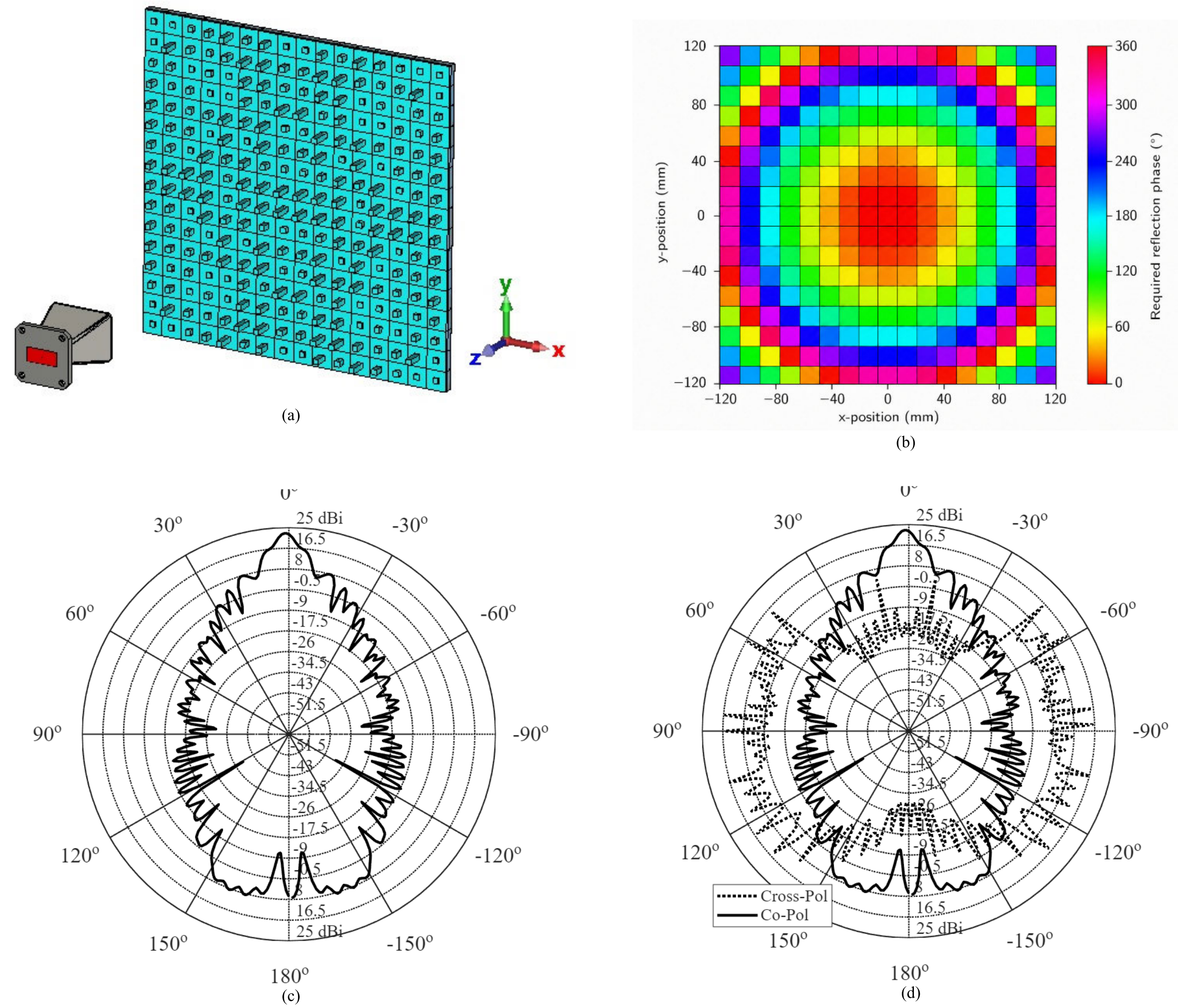

FIGURE 4. 16 × 16 RA designed using the 3D model developed for the unit cell of Fig. 2: (a) 3D view of the RA, (b) computed required reflection-phase map across the aperture at 13 GHz, wrapped into the 0°–360° interval, (c) EM-simulated realized gain at f_0 = 13GHz, and (d) co-polar and cross-polar radiation components.

the aperture through the previously obtained unit-cell phase-response mapping.

A center-fed reflectarray configuration was adopted in this work as a practical baseline geometry for validating the proposed 3D-printed unit-cell concept and aperture-level phase-synthesis procedure. This configuration offers a mechanically simple and symmetric arrangement, facilitates feed-aperture alignment during simulation and measurement, and is well suited for a low-cost proof-of-concept prototype. Although offset-fed reflectarrays can reduce feed blockage and may improve aperture illumination in some cases, they also require more complex asymmetric phase compensation and more demanding mechanical alignment. Therefore, the present work focuses on the center-fed configuration, while the extension of the proposed 3D-printed reflectarray approach to offset-fed and multi-offset arrangements is considered as a future research direction.

The resulting RA configuration is shown in Fig. 4. The aperture is constructed as a 16 × 16 periodic arrangement (i.e., 16 cells along both the x- and y-axes), yielding a total of 256 elements. Figure 4(a) illustrates the three-dimensional model of the full antenna, including the implemented unit-cell layout over the array surface. This layout directly represents the spatially varying phase distribution required to form the targeted reflected wavefront at the operating band.

To validate the aperture-level design, full-wave simulations are carried out and the far-field performance is reported in Fig. 4(c) and Fig. 4(d) at 13 GHz. The figure provides the realized gain and the corresponding radiation characteristics in terms of co-polar and cross-polar components.

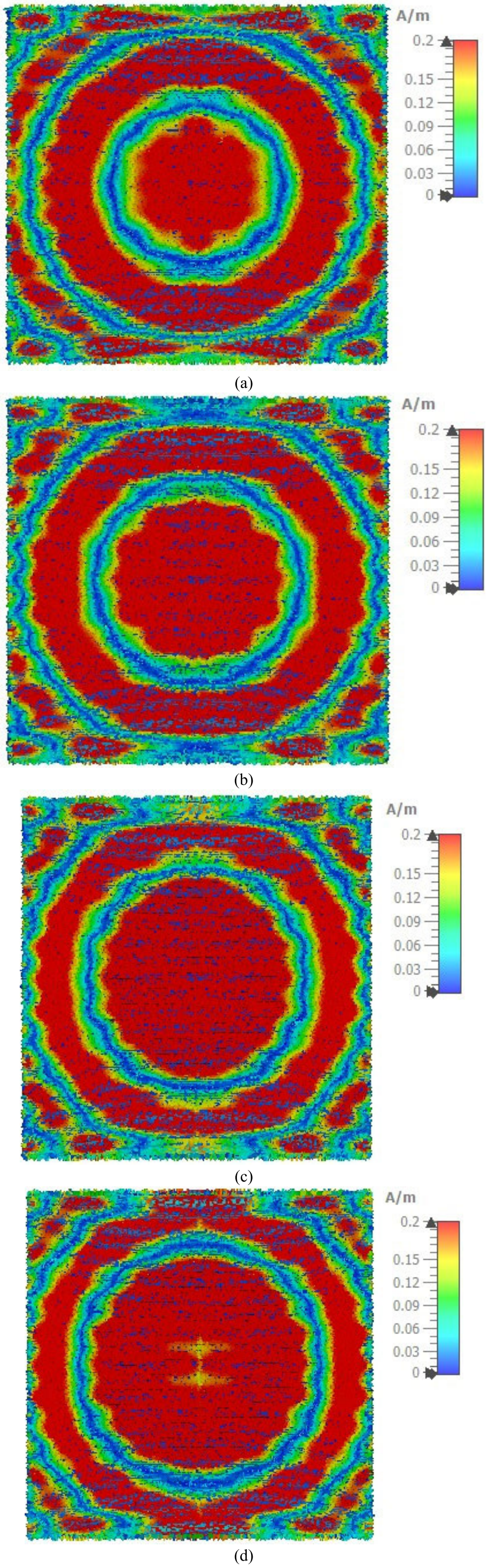

FIGURE 5. Simulated induced surface-current distributions on the RA aperture for different feed excitation-phase references assigned to the horn/feed port in the full-wave simulation: (a) 0°, (b) 30°, (c) 60°, and (d) 90°.

The results confirm that the phase synthesis based on the proposed unit cell enables a directive co-polarized main beam with high gain at the design frequency. In the main-beam region, the co-polarized component remains dominant, indicating that the intended aperture phase distribution is effectively transformed into the desired reflected beam. Overall, the agreement between the intended phase profile and the observed far-field behaviour demonstrates that the proposed unit-cell-driven design procedure effectively scales from the local unit-cell level to the global large-aperture RA implementation.

It should be noted that, although the main-beam region is dominated by the co-polarized component, the cross-polarized field may locally exceed the co-polarized field at certain off-axis angular regions. This behaviour mainly occurs where the co-polarized radiation level is already strongly reduced because of side-lobe or null formation; therefore, it does not represent a dominant cross-polarized main beam. From an electromagnetic perspective, the off-axis cross-polarization can be attributed to the combined effects of oblique feed illumination of the reflectarray aperture, finite-aperture edge diffraction, non-uniform amplitude and phase illumination, and residual higher-order or surface-wave components associated with the 3D dielectric unit-cell geometry. In addition, small fabrication and alignment tolerances may slightly perturb the ideal symmetry of the aperture field and increase the off-axis cross-polarized radiation. For the intended single-polarized Ku-band high-gain communication/RIS-type proof-of-concept considered in this work, this off-axis cross-polarization behaviour is considered acceptable because the useful radiation is concentrated in the co-polarized main-beam direction. However, for dual-polarized radar or other polarization-sensitive applications requiring stringent off-axis polarization isolation, further optimization of the unit-cell symmetry, feed illumination, edge treatment, and polarization-specific aperture synthesis would be necessary.

To further illustrate the aperture-level behaviour, the simulated surface current distribution on the RA is examined for different feed excitation-phase references. In this context, the term feed phase refers to the phase reference assigned to the horn/feed excitation port in the full-wave simulation, and it is not treated as an additional design variable or beam-steering parameter. Figure 5 shows the induced surface-current distributions on the RA aperture when the feed excitation phase is set to 0°, 30°, 60°, and 90°, respectively. These phase cases are used to visualize the current distribution over the aperture at different excitation-phase references. The results indicate that changing the feed excitation phase mainly shifts the phase reference of the induced currents, while the overall current-distribution behaviour remains consistent with the intended reflective operation of the proposed RA.

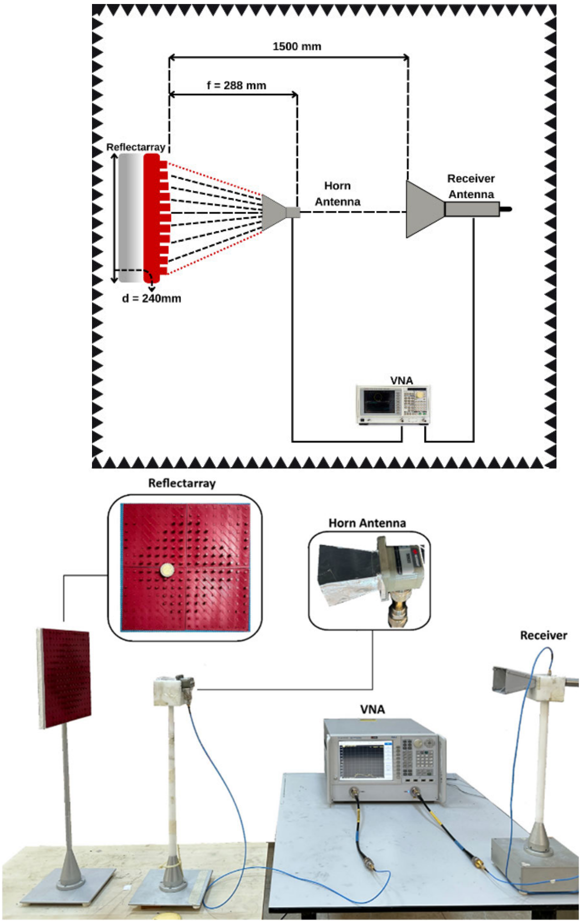

FIGURE 6. **Schematic of the absorber-assisted laboratory measurement setup used for gain characterization of the fabricated center-fed reflectarray. A standard-gain horn antenna, with an approximate gain of 12.5–13.5 dBi around 13 GHz, illuminates the reflectarray at the focal distance f, and the reflected field is received by a second horn connected to the VNA.**

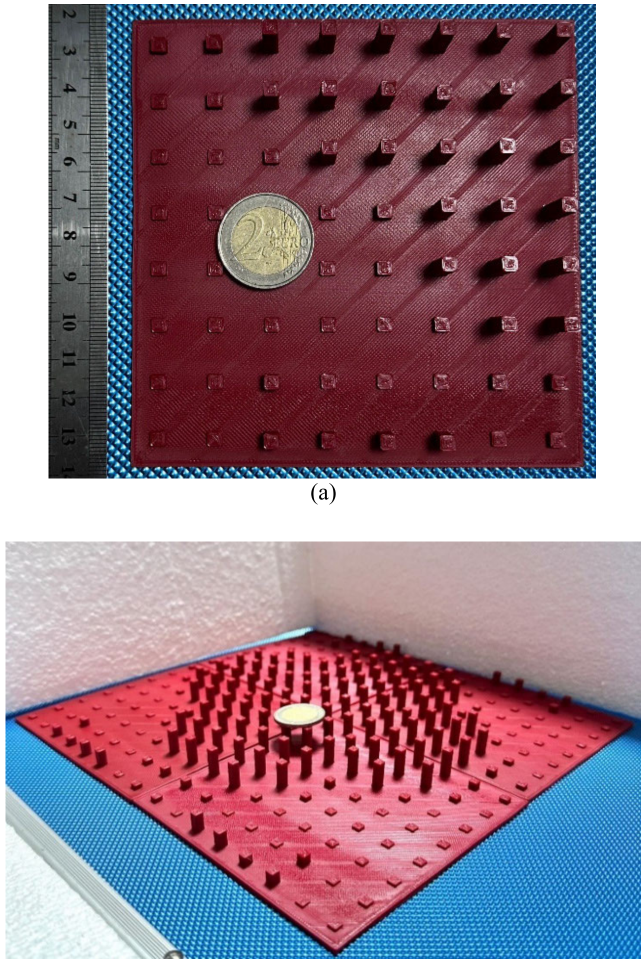

(a)

(b)

FIGURE 7. **Photographs of the fabricated 3D-printed reflectarray prototype: (a) Top View, (b) perspective view of the complete reflectarray.**

TABLE 2. **Simulated and measured EM characteristics of the prototyped RA. Values are reported in simulated/measured format.**

Parameter	12 [GHz]	13 [GHz]	14 [GHz]
Side-Lobe Level	-11.9/-10.8	-13.2/-12.8	-11.7/-13.6
Max Gain [dBi]	21.26/20.4	22.8/21.4	21.9/20.2

IV. EXPERIMENTAL RESULTS

The numerical results presented in the previous sections must be experimentally validated to confirm that the proposed unit-cell–based phase synthesis translates into the expected aperture-level behaviour in practice. Therefore, an experimental campaign is conducted to verify the simulated performance of the fabricated RA prototype.

The overall measurement configuration is schematically illustrated in Fig. 6. A standard-gain horn antenna is used as the feed to illuminate the RA surface. The feed horn has an approximate gain of 12.5–13.5 dBi over the relevant Ku-band frequency range around 13 GHz. The horn is positioned at the designed focal distance f from the RA, corresponding to an f/D ratio of approximately 1.2, where D denotes the side length of the square reflectarray aperture. This f/D value was selected according to the available simulation and measurement setup and was not treated as an independent optimization variable in this work. The selected feed position provides a practical configuration for illuminating the fabricated aperture and forming the reflected wavefront along the desired direction. The reflected field is then captured by a second horn antenna placed in front of the aperture at a larger distance, enabling characterization of the antenna response. Both horn antennas are connected to a vector network analyser (VNA), and the transmission coefficient is recorded to evaluate the reflected signal level and the corresponding realized-gain response. The measurements were not carried out in a fully anechoic chamber; instead, they were performed in a controlled laboratory environment using microwave absorbers placed around the reflectarray, feed horn, receiving horn, and the main reflection regions. This absorber-assisted configuration was used to suppress unwanted reflections and multipath effects as much as possible. The measured results show reasonable agreement with the simulations, indicating that the adopted measurement arrangement was

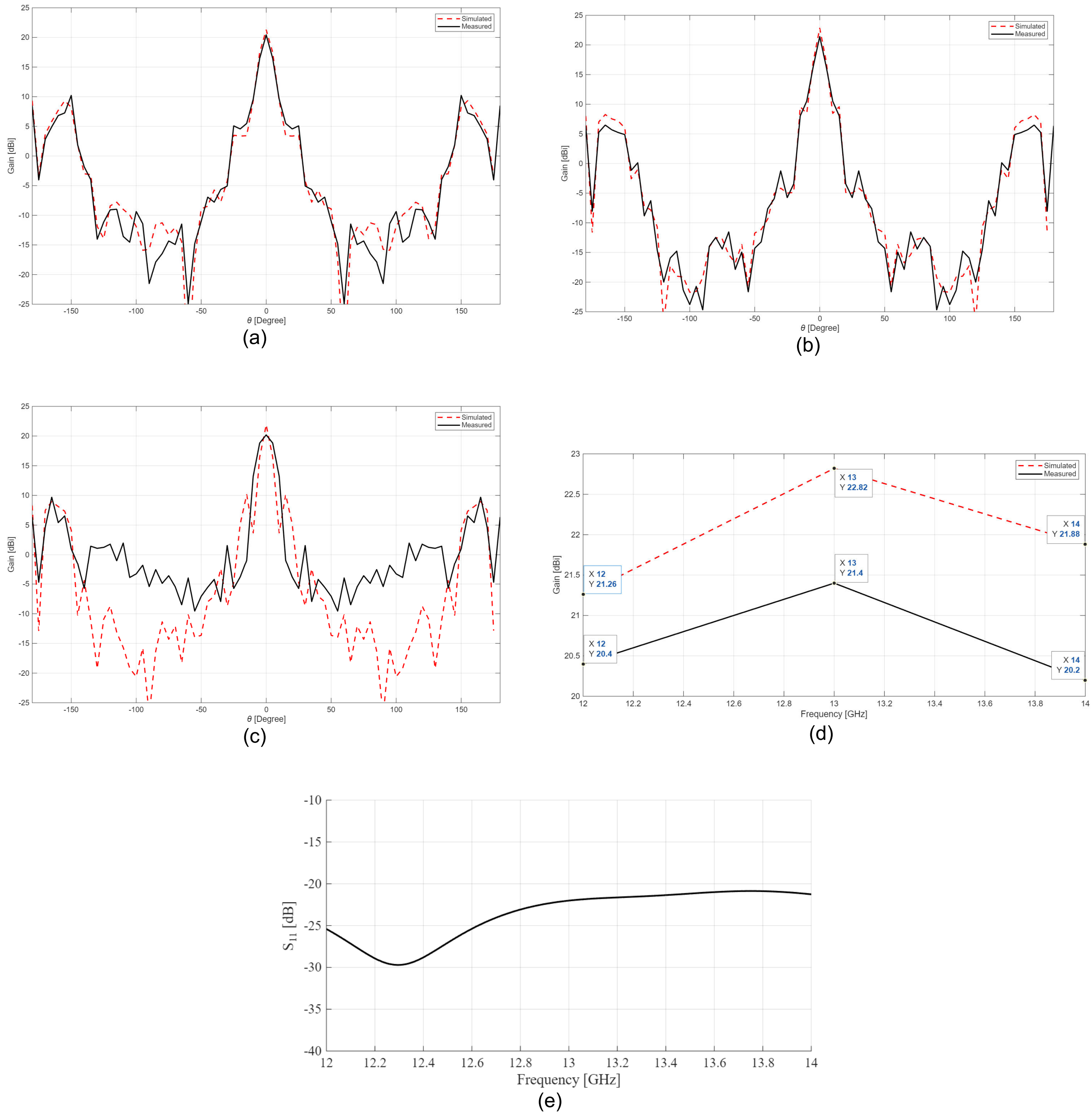

FIGURE 8. **Measured and simulated gain results of the 16 × 16 RA: (a) radiation pattern at 12 GHz, (b) radiation pattern at 13 GHz, (c) radiation pattern at 14 GHz, (d) simulated and measured maximum gain over the operating band, and (e) measured S_{11} over the operating band.**

adequate for validating the proposed reflectarray prototype, although minor residual discrepancies may still arise from environmental reflections, support scattering, non-uniform horn illumination, spillover effects, and alignment tolerances.

Photographs of the fabricated RA are provided in Fig. 7, alongside of the measured performance characteristics in Fig. 8 and Tab. 2. The prototype is realized via 3D printing and subsequently assembled to form the full aperture. From a manufacturing-cost perspective, the proposed prototype benefits from the low material consumption and process simplicity of FDM-based additive manufacturing. The fabricated dielectric reflectarray structure required less than 300 g of PLA filament, corresponding to less than one third of a standard 1 kg filament spool. Therefore, the polymer material cost of the dielectric part remains low. In addition, the proposed fabrication route does not require CNC machining, mold preparation, multilayer PCB lamination, photolithography, or complex subtractive post-processing. Although a full industrial cost analysis depends on local labor, equipment amortization, printer type, and batch size,

TABLE 3. Performance comparison of the proposed RA antenna in the literature for work published in [2011-2019].

Reference	Current Work	[18]	[19]	[20]	[21]	[22]	[23]	[24]	[25]	[29]	[32]	[34]	[35]
Frequency (GHz)	13	8.7-11.2	8.5-11.5	9.1-10.9	12.1-14.8	9.5-12.3	8-12	11.9	---	15	19.7-29.5	19.7	18-20
Number of Layers	1	2	2	1	2	2	1	2	1	2	2	3	2
No. of elements	256	77	52	729	225	277	400	---	400	441	---	625	2242
Aperture Efficiency (%)	10.2	39.8	35	40.3	39	51.3	---	---	13.3	40	---	63	---
Gain (dBi)	21.4	19.3	19	26.1	25	26.4	19.4	24.2	17.8	25.5	45	29.55	36-37
Side-lobe Level	-13	---	-14	-16	-	-17.5	-4	-15	-11.7	-20	-20	SLL_1:-12.36 SLL_2:-11.98	-15
f/D	1.2	1	0.9	1	0.97	0.79	---	1	2.25	0.5	1.5	---	---
Implementation type	3D Printer ε_r:2.1	ε_{r1}:2.65 ε_{r2}: 1.07	ε_{r1}:3.2 ε_{r2}: 1.07	ε_r:2.2	ε_{r1}:3.55 ε_{r2}: 1	ε_{r1}:3.48 ε_{r2}: 1	ε_r:1.98	ε_{r1}: 3.4 ε_{r2}: 1	ε_r: 2.2	ε_r:2.2	ε_{r1}:2.3 ε_{r2}:2.17	ε_{r1}:2.3 ε_{r2}:2.32 ε_{r3}:2.17	ε_{r1}:2.17 ε_{r2}:2.33
Size (mm)	240x240	140x140	12.5x125	270x270	180x180	285x285	400x400	288x288	200x200	189x189	0.777x0.706	180x180	427,5 x 425

TABLE 4. Performance comparison of the proposed RA antenna in the literature for work published in [2020-2026].

Reference	Current Work	[26]	[27]	[28]	[29]	[31]	[36]
Frequency (GHz)	13	8	10.1	9.85	12.5	20-30	5.84
Number of Layers	1	2	2	2	2	2	1
No. of elements	256	286	144	144	256	1296	280
Aperture Efficiency (%)	10.2	38.9	21.45	28	15.4	39.1-41.3	13.6
Gain (dBi)	21.4	20	16.64	17.14	20.5	28.5-32.25	18
Side-lobe Level	-13	-8	-9.24 -10.43	-12.5	-	---	---
f/D	1.2	0.51	0.36	0.36	0.86	---	0.37
Implementation type	3D Printer ε_r:2.1	ε_r:3.55	ε_r:2.2	ε_r:2.2	ε_{r1} :2.55 ε_{r2} :10.2	Chemical Photoetching ε_r:2.17	Origami
Size (mm)	240x240	217x208	126x126	126 x 73.32	192x192	180x180	500x500

the present prototype demonstrates a low-material-cost and low-complexity route for rapid reflectarray prototyping. Similar cost-effectiveness and fabrication-simplicity advantages of additive manufacturing for antenna applications have also been reported in the literatures [15], [16], and [17]. A reference object is included in the photos to provide a clear sense of scale, and the assembled structure demonstrates the intended spatial variation across the surface that implements the required phase distribution. The measured results reported in this section are used to directly validate the simulation-based design, demonstrating the feasibility of the proposed approach for large-aperture RA implementations.

The relatively low aperture efficiency of the proposed reflectarray is mainly attributed to the feed-aperture illumination condition rather than to the intrinsic loss of the 3D-printed unit cell alone. For the implemented center-fed configuration, the aperture side length is D = 240 mm and the selected feed distance corresponds to f/D $\approx$ 1.2, i.e., f $\approx$ 288 mm. Therefore, the reflectarray aperture subtends an angle of approximately 22.6° toward the aperture edge and 30.5° toward the diagonal direction as observed from the feed phase center. Using the feed-horn radiation pattern/approximation, the spillover efficiency, defined as the fraction of the feed-radiated power intercepted by the finite reflectarray aperture, was estimated to be approximately 0.55–0.67 around 13 GHz. This indicates that a non-negligible portion of the feed power is radiated outside the useful aperture region and therefore does not contribute to the phase-corrected reflected beam. Consequently, the overall realized gain and aperture efficiency are reduced, and part of the undesired radiation may also contribute to residual back-lobe and scattering effects in the measurement environment. This limitation can be mitigated in future design iterations by optimizing the feed position and illumination taper, increasing the aperture size, adopting an offset-fed configuration to reduce blockage and improve illumination control, or employing choke-ring/edge-treatment structures to suppress spillover and edge diffraction. Although the measured radiation response confirms the expected directive behaviour of the proposed reflectarray, a residual back-lobe component can still be observed in the measured pattern. This behaviour is mainly attributed to practical measurement and implementation effects, including the finite aperture size of the fabricated prototype, edge diffraction from the reflectarray boundary, non-ideal feed illumination, and scattering from the supporting fixture and surrounding measurement arrangement. In addition, small fabrication and alignment tolerances may slightly disturb the ideal aperture phase distribution, contributing to increased radiation in the backward direction. Nevertheless, the dominant main-beam response and the overall agreement between simulation and measurement indicate that the proposed phase-synthesis and fabrication approach remains valid.

To highlight the achieved performance of the proposed RA and to position the contribution with respect to the state of the art, Tables 3 and 4 provides a quantitative comparison between the current work and 13 representative RA antennas reported in the literature. The comparison includes key design and performance indicators, namely the operating frequency, number of layers, number of elements, aperture efficiency, realized gain, side-lobe level (SLL), f/D ratio, and the adopted fabrication/technology (including dielectric properties).

As summarized in Tabs. 3 and 4, the proposed RA operates at 13 GHz and employs a single-layer configuration with 256 elements, implemented via 3D printing using PLA with $\varepsilon r \approx 2.1$. The antenna achieves a simulated realized gain of 21.4 dBi and an aperture efficiency of 10.2% at 13 GHz. The obtained gain is comparable to several reported single- and multilayer reflectarray designs, particularly considering the structurally simple single-layer implementation and the moderate number of elements used in the proposed aperture. The f/D ratio was determined from the implemented horn-fed reflectarray geometry, where f denotes the feed-to-aperture distance and D denotes the side length of the square reflectarray aperture. In this work, f/D=1.2 was selected according to the available simulation and measurement setup, rather than being treated as an independent optimization variable. This value provides a practical feed position for illuminating the fabricated aperture and remains within the range of values reported in comparable reflectarray studies. Spillover efficiency refers to the fraction of the feed-radiated power intercepted by the finite reflectarray aperture. Therefore, non-ideal horn illumination, spillover loss, edge diffraction, finite-aperture effects, and practical fabrication/alignment tolerances are considered among the main factors contributing to the obtained aperture-efficiency value. The comparison also indicates that aperture efficiency and SLL are not consistently reported across all studies, which underlines the practical value of presenting multiple metrics together in a single benchmark. Overall, this comparison demonstrates that the proposed design offers a favourable performance–complexity trade-off, achieving Ku-band operation with a structurally simple, single-layer, additively manufactured RA implementation.

V. CONCLUSION

This paper presented the design, fabrication, and experimental validation of a Ku-band 3D-printed RA antenna operating at 13 GHz. The proposed architecture employs a PLA-based multilayer unit cell incorporating an air spacer and a square-ring resonator to achieve continuous reflection-phase control through geometry–material co-optimization. A systematic parametric investigation revealed that the air-gap thickness provides the primary phase-tuning mechanism, while dielectric thickness, permittivity, and resonator dimensions enable precise secondary control. This layered phase-synthesis strategy establishes a scalable and fabrication-aware framework for additive-manufactured RA. A 16×16 aperture composed of 256 elements (240×240 mm^2) was synthesized using full-wave–derived phase mapping and classical compensation theory. Numerical results demonstrated a realized gain of 21.4 dBi at 13 GHz with controlled sidelobe levels and stable main-beam polarization characteristics. Although local off-axis cross-polarization enhancement is observed in angular regions where the co-polarized field is already weak, the main-beam response remains suitable for the intended single-polarized Ku-band proof-of-concept; nevertheless, future dual-polarized or radar-oriented implementations would require dedicated polarization-isolation optimization. The fabricated prototype, characterized using a horn-fed measurement setup, showed good agreement with simulations, confirming both the predictive accuracy of the unit-cell phase model and the robustness of the proposed design methodology.

Beyond demonstrating a single high-gain prototype, this work contributes a reproducible and manufacturable design pipeline for low-cost Ku-band RA. The exclusive reliance on additive manufacturing significantly reduces fabrication complexity and enables rapid prototyping, geometric customization, and lightweight implementations suitable for satellite terminals, UAV platforms, and portable high-frequency communication systems. From a forward-looking perspective, the presented framework can be directly extended toward larger apertures for higher gain, multi-band or broadband configurations through stacked or dispersion-engineered unit cells, and polarization-agile designs. Moreover, the geometrically controlled phase mechanism is inherently compatible with the integration of tunable components (e.g., varactors, liquid crystals, or printed conductive inks), paving the way for reconfigurable RA and software-defined beam steering. This positions the proposed architecture as a practical stepping stone toward low-cost reconfigurable intelligent surfaces (RIS) operating in the Ku band and beyond. In summary, the results confirm that 3D-printing–based RA technology can move beyond proof-of-concept demonstrations toward scalable, adaptive, and system-integrable high-frequency platforms, aligning with the evolving demands of next-generation satellite and intelligent wireless communication infrastructures.

REFERENCES

[1] J. Huang and J. A. Encinar, *Reflectarray Antennas: Theory, Designs, and Applications*. Hoboken, NJ, USA: Wiley, 2007.

[2] K. K. Karnati, Y. Yusuf, S. Ebadi, and X. Gong, "Theoretical analysis on reflection properties of reflectarray unit cells using quality factors," *IEEE Trans. Antennas Propag.*, vol. 61, no. 1, pp. 201–210, Jan. 2013.

[3] S. Koziel, M. A. Belen, A. Çalışkan, and P. Mahouti, "On direct EM-driven optimization of reflectarray antennas for gain enhancement and sidelobe suppression," *IEEE Trans. Antennas Propag.*, 2025, doi: 10.1109/TAP.2025.3618757.

[4] Y. Yang, Y. Su, Y. Liu, M. Li, S. Wu, X. Q. Lin, B. Zhang, and Y. Fan, "A single-layer dual-band dual-polarizied shared-aperture metasurface composed of antenna array and reflectarray," *IEEE Antennas Wireless Propag. Lett.*, vol. 25, no. 4, pp. 1462–1466, Apr. 2026, doi: 10.1109/LAWP.2026.3656948.

[5] Y. S. Gurbet and S. Doğu, "Comprehensive review of Ku, K, and Ka band antenna designs: Applications in CubeSats," *Int. J. Aeronaut. Space Sci.*, vol. 27, no. 1, pp. 447–496, Jan. 2026.

[6] Y. Yang, Y. Su, Y. Yao, M. Li, S. Wu, X. Q. Lin, B. Zhang, and Y. Fan, "Low-profile tri-band shared-aperture metasurface used for C-band phased array and K/Ka-band reflectarray," *IEEE Trans. Antennas Propag.*, vol. 74, no. 5, pp. 4389–4400, May 2026.

[7] F. Ahmed, F. Faisal, N. Melouki, P. PourMohammadi, H. Naseri, T. Djerafi, and T. A. Denidni, "A wideband water-based 3D-printed reflect–transmit antenna array toward mmWave positioning applications," *Sensors*, vol. 26, no. 4, p. 1249, Feb. 2026.

[8] M. A. Belen, A. Caliskan, S. Koziel, A. Pietrenko-Dabrowska, and P. Mahouti, "Optimal design of transmitarray antennas via low-cost surrogate modelling," *Sci. Rep.*, vol. 13, no. 1, p. 15044, Sep. 2023.

[9] P. Mahoutı, F. Güneş, M. A. Belen, and A. Çalışkan, "A novel design of non-uniform reflectarrays with symbolic regression and its realization using 3-D printer," *ACES J.*, vol. 34, no. 2, pp. 280–285, Feb. 2019.

[10] S. Koziel, M. A. Belen, A. Çaliskan, and P. Mahouti, "Rapid design of 3D reflectarray antennas by inverse surrogate modeling and regularization," *IEEE Access*, vol. 11, pp. 24175–24184, 2023, doi: 10.1109/ACCESS.2023.3254204.

[11] P. Nayeri, F. Yang, and A. Z. Elsherbeni, *Reflectarray Antennas: Theory, Designs, and Applications*. Hoboken, NJ, USA: Wiley, Feb. 2018.

[12] A. Belen, F. Güneş, M. A. Belen, and P. Mahouti, "3D printed wideband flat gain multilayer nonuniform reflectarray antenna for X-band applications," *Int. J. Numer. Model., Electron. Netw., Devices Fields*, vol. 33, no. 6, p. e2753, Nov. 2020.

[13] A. A. Mugheri, M. I. Abbasi, I. M. Ibrahim, S. H. Kiani, M. H. Dahri, M. R. Kamarudin, Z. A. Shamsan, and Q. H. Abbasi, "Recent advances in transparent reflectarray antennas," *IEEE Access*, vol. 13, pp. 161541–161572, 2025, doi: 10.1109/ACCESS.2025.3607095.

[14] F. Xue, M. Fu, Z. Li, G. Feng, H. Chen, and Y. Li, "Reconfigurable dual-band circularly polarized reflectarray with small frequency ratio incorporating precoding technology," *IEEE Trans. Antennas Propag.*, vol. 74, no. 5, pp. 4909–4914, May 2026.

[15] M. Aziz, A. El Hassan, M. Hussein, E. Zaneldin, A. H. Al-Marzouqi, and W. Ahmed, "Characteristics of antenna fabricated using additive manufacturing technology and the potential applications," *Heliyon*, vol. 10, no. 6, Mar. 2024, Art. no. e27785, doi: 10.1016/j.heliyon.2024.e27785.

[16] Á. F. Vaquero, A. Rebollo, and M. Arrebola, "Additive manufacturing in compact high-gain wideband antennas operating in mm-wave frequencies," *Sci. Rep.*, vol. 13, no. 1, p. 10998, 2023, doi: 10.1038/s41598-023-38247-x.

[17] S. Alkaraki, Z. Ullah Khan, S. F. Jilani, A. Andre Sarker, J. R. Kelly, and A. Alomainy, "Low–cost 3D–printed standard gain horn antennas for millimetre–wave applications," *J. Manuf. Mater. Process.*, vol. 9, no. 7, p. 222, Jul. 2025, doi: 10.3390/jmmp9070222.

[18] L.-S. Ren, Y.-C. Jiao, F. Li, J.-J. Zhao, and G. Zhao, "A novel double-petal loop element for broadband reflectarray," *Prog. Electromagn. Res. Lett.*, vol. 20, pp. 157–163, 2011.

[19] -J.-J. Zhao, -S.-X. Gong, -Y.-X. Xu, and -L.-S. Ren, "Design of a broadband reflectarray using meander-shaped elements," *Microw. Opt. Technol. Lett.*, vol. 54, pp. 500-503, 2012. [Online]. Available: https://doi.org/10.1002/mop.26563

[20] J. Wu, X. Da, K. Wu, and Y. Liang, "Circularly polarized high efficiency wideband reflectarray using rectangle-shaped patch element," *Int. J. RF Microw. Comput.-Aided Eng.*, vol. 27, no. 5, Jun. 2017, Art. no. e21089.

[21] S. F. Qotolo, H. R. Hassani, and M. Naser-Moghadasi, "A novel broadband reflectarray antenna with lattice stubs on square element for Ku-band application," *Microw. Opt. Technol. Lett.*, vol. 57, no. 11, pp. 2699–2702, Nov. 2015.

[22] C. Han, Y. Zhang, and Q. Yang, "A novel single-layer unit structure for broadband reflectarray antenna," *IEEE Antennas Wireless Propag. Lett.*, vol. 16, pp. 681–684, 2017.

[23] S. Rouzbahani, A. Z. Nezhad, and M. M. Ali, "Design of reflectarray with cosecant squared radiation pattern in X-band," in *Proc. 24th Iranian Conf. Electr. Eng. (ICEE)*, Shiraz, Iran, May 2016, pp. 502–506.

[24] H. Luyen, Z. Yang, M. Gao, J. H. Booske, and N. Behdad, "A wideband, single-layer reflectarray exploiting a polarization rotating unit cell," *IEEE Trans. Antennas Propag.*, vol. 67, no. 2, pp. 872–883, Feb. 2019.

[25] S.-W. Qu, Q.-Y. Chen, M.-Y. Xia, and X. Y. Zhang, "Single-layer dual-band reflectarray with single linear polarization," *IEEE Trans. Antennas Propag.*, vol. 62, no. 1, pp. 199–205, Jan. 2014.

[26] W. Li, H. Tu, Y. He, L. Zhang, S.-W. Wong, and S. Gao, "A novel wideband tightly coupled dual-polarized reflectarray antenna," *IEEE Trans. Antennas Propag.*, vol. 71, no. 6, pp. 5422–5427, Jun. 2023, doi: 10.1109/TAP.2023.3262969.

[27] Y.-H. Nam, Y. Kim, S.-G. Lee, and J.-H. Lee, "Hybrid reflectarray antenna of passive and active unit cells for highly directive two-direction beam steering," *IEEE Access*, vol. 11, pp. 6299–6304, 2023, doi: 10.1109/ACCESS.2022.3232120.

[28] S.-G. Lee, Y.-H. Nam, Y. Kim, J. Kim, and J.-H. Lee, "A wide-angle and high-efficiency reconfigurable reflectarray antenna based on a miniaturized radiating element," *IEEE Access*, vol. 10, pp. 103223–103229, 2022, doi: 10.1109/ACCESS.2022.3204400.

[29] W. Su, W. Luo, Z. Nie, W.-W. Liu, Z.-H. Cao, and Z. Wang, "A wideband folded reflectarray antenna based on single-layered polarization rotating metasurface," *IEEE Access*, vol. 8, pp. 158579–158584, 2020, doi: 10.1109/ACCESS.2020.3019822.

[30] B. Xi, Y. Xiao, K. Zhu, Y. Liu, H. Sun, and Z. Chen, "1-bit wideband reconfigurable reflectarray design in Ku-band," *IEEE Access*, vol. 10, pp. 4340–4348, 2022, doi: 10.1109/ACCESS.2021.3117693.

[31] M. Abdollahvand, K. Forooraghi, J. A. Encinar, Z. Atlasbaf, and E. Martinez-de-Rioja, "A 20/30 GHz reflectarray backed by FSS for shared aperture Ku/Ka-band satellite communication antennas," *IEEE Antennas Wireless Propag. Lett.*, vol. 19, no. 4, pp. 566–570, Apr. 2020, doi: 10.1109/LAWP.2020.2972024.

[32] D. Martinez-de-Rioja, E. Martinez-de-Rioja, J. A. Encinar, A. Pino, Y. Rodriguez-Vaqueiro, B. Gonzalez-Valdes, O. Rubiños, and M. Arias, "Single and dual reflectarray configurations for multibeam satellite antennas in Ka-band," in *Proc. 13th Eur. Conf. Antennas Propag. (EuCAP)*, Krakow, Poland, Mar. 2019, pp. 1–5.

[33] A. Somolinos, R. Florencio, I. González, J. A. Encinar, and F. Cátedra, "Experimental validation of generating two spaced beams with reflectarrays by VRT," *IEEE Trans. Antennas Propag.*, vol. 67, no. 6, pp. 4263–4268, Jun. 2019, doi: 10.1109/TAP.2019.2907862.

[34] R. Florencio, J. A. Encinar, R. R. Boix, M. Barba, and G. Toso, "Flat reflectarray that generates adjacent beams by discriminating in dual circular polarization," *IEEE Trans. Antennas Propag.*, vol. 67, no. 6, pp. 3733–3742, Jun. 2019, doi: 10.1109/TAP.2019.2905676.

[35] D. Martinez-De-Rioja, E. Martinez-De-Rioja, J. A. Encinar, R. Florencio, and G. Toso, "Reflectarray to generate four adjacent beams per feed for multispot satellite antennas," *IEEE Trans. Antennas Propag.*, vol. 67, no. 2, pp. 1265–1269, Feb. 2019, doi: 10.1109/TAP.2018.2880117.

[36] K. Suzuki, H. Kurokawa, G. Nakayama, M. Yasuhara, A. Ochi, S. So Yeon, H. Sakamoto, and T. Tomura, "A 5.8-GHz-band origami deployable reflectarray antenna for CubeSats," *IEEE Trans. Antennas Propag.*, vol. 74, no. 4, pp. 3142–3153, Apr. 2026, doi: 10.1109/TAP.2026.3656735.

LADISLAU MATEKOVITS (Senior Member, IEEE) received the degree in electronic engineering from the Institutul Politehnic din Bucureşti, Bucureşti, Romania, in 1992, and the Ph.D. (Dottorato di Ricerca) degree in electronic engineering from the Politecnico di Torino, Turin, Italy, in 1995.

Since 1995, he has been with the Department of Electronics and Telecommunications, Politecnico di Torino, first with a post-doctoral fellowship and then as a Research Assistant. He joined the Department of Electronics and Telecommunications as an Assistant Professor, in 2002, where he was appointed as a Senior Assistant Professor, in 2005, and an Associate Professor, in 2014. In February 2017, he was a Full Professor (Italy). In Late 2005, he was a Visiting Scientist at the Antennas and Scattering Department, FGAN-FHR (now Fraunhofer Institute), Wachtberg, Germany. In July, 2009, he was a Marie Curie Fellow at Macquarie University, Sydney, NSW, Australia, for two years, where he also held a visiting academic position, in 2013, and was appointed as an Honorary Fellow, in 2014. Since 2020, he has been an Honorary Professor with the Polytechnic University of Timisoara, Romania, and an Associate Professor of Italian National Research Council. He has published more than 500 articles, including more than 155 journal contributions, and delivered seminars on these topics all around the world: Europe, USA (AFRL/MIT-Boston), Australia, China, and Russia. He has been invited to serve as a Research Grant Assessor for government funding calls (Romania, Italy, Croatia, and Kazakhstan) and as an International Expert in Ph.D. thesis evaluation by several universities from Australia, India, Pakistan, and Spain. His research interests include the numerical analysis of printed antennas and, in particular, the development of new, numerically efficient full-wave techniques to analyze large arrays, optimization techniques, and active and passive metamaterials for cloaking applications. Material parameter retrieval of these structures by inverse methods and different optimization techniques have also been considered. In recent years, bio-electromagnetic aspects have also been contemplated, for example, the design of implantable antennas or development of nano-antennas, for example, for drug delivery applications.

Prof. Matekovits has been a member of the Organizing Committee of the International Conference on Electromagnetics in Advanced Applications (ICEAA), since 2010. He is a member of the technical program committee of several conferences. He has been a recipient of various awards in international conferences, including the 1998 URSI Young Scientist Award, Thessaloniki, Greece; the 1998 Barzilai Award (Young Scientist Award, granted every two years by Italian National Electromagnetic Group); and the Best AP2000 Oral Paper on Antennas, ESA-EUREL Millennium Conference on Antennas and Propagation, Davos, Switzerland. He was a recipient of the 2018 Motohisa Kanda Award, for the most cited paper of the IEEE Transactions on Electromagnetic Compatibility in the past five years, and more recently he has been awarded with the 2019 American Romanian Academy of Arts and Sciences (ARA) Medal of Excellence in Science and by the 2020 Ad Astra Award and a Senior Researcher for Excellence in Research. He has been the Assistant Chairperson and the Publication Chairperson of the 2002 European Microwave Week, Milan, Italy; and General Chair of the 11th International Conference on Body Area Networks (BodyNets), in 2016. He serves as an Associate Editor for IEEE Access, IEEE Antennas and Wireless Propagation Letters, and IET MAP; and a reviewer for different journals.

FURKAN BAŞKıR received the B.Sc. degree in electrical and electronics engineering from İskenderun Technical University, Türkiye. His research interests include reconfigurable intelligent surfaces, frequency-selective surfaces, reflectarray and transmitarray antennas, metasurface-based antenna systems, and electromagnetic optimization techniques. He has been involved in several research activities related to advanced antenna design, including projects on radar cross-section reduction and 3-D-printed multi-layer phase-shifting transmitarray antennas for radar applications.

HASAN KıYıK received the M.Sc. degree in aeronautical and astronautical engineering from Istanbul Technical University, in 2020. He is currently a System Installation Design Chief Engineer with Turkish Aerospace. He specializes in finite element methods, structural optimization, and the static and dynamic analysis of aerospace structures.

AYSU BELEN received the M.Sc. degree in electronics and communication engineering from the Yıldız Technical University, in 2016. She is currently an Assistant Professor with İskenderun Technical University. Her research interests include optimization of microwave circuits, device modeling, computer-aided circuit design, and microwave amplifiers.

TARLAN MAHOUTI received the B.Sc. and M.Sc. degrees in metallurgy and materials science engineering from Yıldız Technical University, in 2018 and 2022, respectively, where she is currently pursuing the Ph.D. degree, with a focus on artificial intelligence, polymer–nanocomposite material development, dielectric materials, material characterization, antenna design, and phantom development. She has also worked on material and system modeling, simulation and validation, and the development of AI algorithms for design optimization.

MEHMET ALI BELEN received the Ph.D. degree in electronics and communication engineering from Yıldız Technical University, in 2016. He is currently a Professor with İskenderun Technical University. His current research interests include the areas of multivariable network theory, device modeling, computer-aided microwave circuit design, monolithic microwave integrated circuits, and antenna arrays, active/passive microwave components, especially in the field of metamaterial-based antennas and microwave filters.